

Highly Luminescent Liquid Crystals in Aggregation Based on Platinum(II) Complexes

Xingtian Hao, Bijin Xiong, Mingli Ni, Bing Tang, Ying Ma, Haiyan Peng,* Xingping Zhou, Ivan I. Smalyukh, and Xiaolin Xie*



Cite This: <https://dx.doi.org/10.1021/acsami.0c13935>



Read Online

ACCESS |



Metrics & More



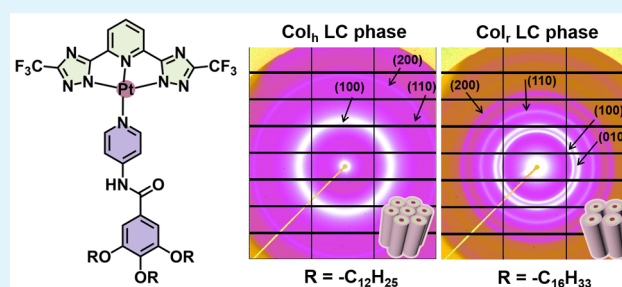
Article Recommendations



Supporting Information

ABSTRACT: Luminescent liquid crystals (LLCs) attract considerable attention because of their broad applications in displays, chemosensors, and anti-counterfeiting. However, it remains challenging to achieve a high luminescence efficiency in LCs because of the common aggregation-caused quenching effect. Herein, we demonstrate a facile approach to designing LLCs with a high quantum yield up to 88% by deliberately tuning the aggregation behavior of platinum(II) complexes with alkoxy chains ($C_nH_{2n+1}O-$). LLCs in hexagonal columnar and rectangular columnar phases are achieved when $n = 12$ and 16, respectively, as revealed by one-dimensional wide-angle X-ray diffraction and small-angle X-ray scattering. These LLCs are able to not only exhibit strong emission at elevated temperatures but also show attractive reversible vapochromism upon alternative CH_2Cl_2 and EtOH fuming, which imparts added functions and promises technological utility.

KEYWORDS: liquid crystals, platinum(II) complexes, luminescence, aggregation, vapochromism, chemosensors, anti-counterfeiting, metal...metal interactions



INTRODUCTION

Luminescent liquid crystals (LLCs), which exhibit attractive photoluminescence and mesophase behaviors, have drawn considerable attention because of their great potential for applications in displays,¹ organic light-emitting diodes,² and field-effect transistors.³ Very recently, LLCs have also been patterned for anti-counterfeiting⁴ through holographic photopolymerization-induced phase separation.^{5–9} Nevertheless, it still remains a formidable challenge to design LLCs with a high photoluminescence efficiency because of the inherent aggregation-caused quenching (ACQ) effect of the common LC luminophores.^{10,11}

As a solution, it would be reasonable to design LLCs based on AIEgens (i.e., aggregation-induced emission luminogens), because AIEgens are able to exhibit much brighter emission with the increase of the aggregation and, thus, could allow one to tackle the challenges related to the ACQ.^{12–14} To this end, AIEgens such as tetraphenylethene,^{15–19} cyanostilbene,^{20–22} tolane,²³ silole,²⁴ and thiophene²⁵ have been employed to design LLCs. Nonetheless, the absolute quantum yield (QY) of these LLCs based on organic AIEgens is still lower than 60% and LLCs with much higher QY are limited.¹⁷

To address this hurdle, platinum(II) complexes, that are shorted as Pt(II) complexes, come to our attention because of their much higher QY after molecular aggregation.^{26–28} The square-planar geometry of Pt(II) complexes is in favor of their

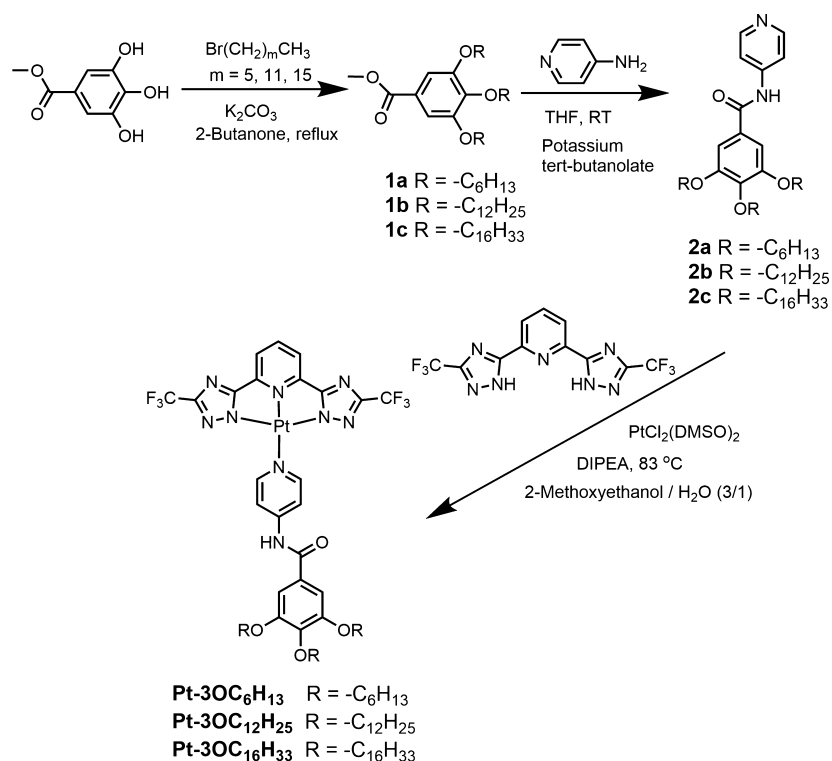
stacking in the aggregated states through intermolecular Pt...Pt and $\pi-\pi$ interactions,²⁹ which promises LC properties by means of tuning the aggregation behaviors. Furthermore, the Pt...Pt distance can be greatly reduced when meeting with volatile organic compounds (VOCs), giving rise to a redshifted emission by metal-metal-ligand charge transfer (MMLCT).³⁰ More excitingly, the emission color can go back to the original one after getting rid of the VOCs. Therefore, Pt(II) complexes show a great application potential in reusable chemosensors and advanced anti-counterfeiting. It is also reported that Pt(II) complexes are able to exhibit outstanding electrochemiluminescence properties, promising the development of new emitters for advanced biosensing and immuno-assaying.²⁶ Nonetheless, only a few LLCs based on Pt(II) complexes have been reported.^{3,31–34} For instance, Bruce and co-workers have reported columnar mesophases based on the tridentate N,C,N-coordinated Pt(II) complexes with a QY of 12%.³¹ Lodeiro and co-workers have developed multistimuli-responsive LLCs sensitive to temperature, pressure, and VOCs based on

Received: August 3, 2020

Accepted: October 28, 2020



Scheme 1. Illustration on the Synthesis of Pt(II) Complexes



unsymmetrically four-coordinated Pt(II) complexes, with the associated QY of 20%.³² Che,³ Ziessel,³³ and co-workers have reported lyotropic LLCs and thermotropic LLCs based on cationic Pt(II) complexes, though their QY is unknown. Hereto, the QY of LLCs based on Pt(II) complexes is still low except for that (86%) of the cationic cyclometalated Pt(II) complexes reported by Swager and co-workers.³⁴ The high QY in this case is ascribed to the special molecular arrangement mediated by the intermolecular hydrogen bonding interactions.

Herein, we demonstrate a different and robust approach to designing LLCs with high QY up to 88%, by tuning the aggregation behaviors of Pt(II) complexes with alkoxy chains. Highly ordered columnar structures are expected in the assembled Pt(II) complexes because of the greatly boosted intermolecular Pt··Pt and π - π interactions by the square-planar core geometry. On the other hand, distinct mesophases, that is, hexagonal columnar (Col_h) and rectangular columnar (Col_r) phases are achieved by predesigned modifications of the complex core with different flexible peripheral alkoxy chains (e.g., dodecyloxy and hexadecyloxy chains).

EXPERIMENTAL SECTION

Materials and Characterization. Methyl gallate (purity: 98%), trifluoroacetic anhydride (purity: 99%), and diethylene glycol dimethyl ether (diglyme, purity: 99%) were purchased from Adamas Reagent Co., Ltd., China. 2,6-Pyridinedicarbonitrile (purity: 97%) was received from Ark Pharm, United States. 1-Bromohexane (purity: 98%), 1-bromododecane (purity: 98%), 1-bromohexadecane (purity: 97%), and 4-aminopyridine (purity: 98%) were obtained from Aladdin, China. Potassium tetrachloroplatinate(II) (purity: 99%), *N,N*-diisopropylethylamine (DIPEA, purity: 99%), and potassium *tert*-butanolate (purity: 98%) were obtained from Beijing Innochem Science & Technology Co., Ltd., China. Potassium carbonate (K_2CO_3 , AR), 2-methoxyethanol (purity: 99%), hydrazine monohydrate ($\text{NH}_2\text{NH}_2 \cdot \text{H}_2\text{O}$), concentrated hydrochloric acid (HCl), tetrahydrofuran (THF), dichloromethane (DCM), ethanol (EtOH),

dimethylsulfoxide (DMSO), 2-butanone, petroleum ether, and diethyl ether were acquired from Sinopharm Chemical Reagent Co., Ltd., China. Calcium hydride (CaH_2 , purity: 98%) was purchased from Energy Chemical Co., Ltd., China. THF was purified via distillation under vacuum after stirring for 2 h in the presence of CaH_2 . Deionized water was obtained through purification on one ultrapure water machine (CS-5, Wuhan Jibari Technology Co., Ltd., China).

Column chromatography was performed on a 200–300 mesh silica gel to purify the synthesized products. Nuclear magnetic resonance (e.g., ^1H NMR, ^{13}C NMR, and ^{19}F NMR) spectra were recorded on a 400 or 600 MHz spectrometer (Ascend, Bruker, Germany) with tetramethylsilane as the internal standard. Elemental analysis was performed on an element analyzer (Vario Microcube, Elementar, Germany). High-resolution mass spectrometry studies were implemented with FT-MS (Solarix 7.0T, Bruker Daltonics, United States). The thermal stability was evaluated on a thermogravimetric analyzer (TGA 4000, PerkinElmer, United States) at a ramp rate of 10 °C/min from 30 to 800 °C. Phase transition temperatures were measured by differential scanning calorimetry (DSC, Q2000, TA Instruments, United States) at a ramp rate of 5 °C/min. Polarized optical microscopy (POM) images were captured using a microscope (Axio Scope. A1, Carl Zeiss, Germany) that was equipped with a hot stage (THMS 600, Linkam, United Kingdom). Optical images were taken when cooling the isotropic liquid samples to room temperature at a ramp rate of 5 °C/min. Small-angle X-ray scattering (SAXS) characterizations were carried out using the BL16B1 beamline at the Shanghai Synchrotron Radiation Facility (SSRF), China. UV–vis absorption spectra were recorded using a spectrometer (Evolution 220, Thermo Fisher, United States). The emission spectra, absolute QY, and lifetime were measured on a spectrofluorometer (FLS1000, Edinburgh Instruments, United Kingdom). Powder X-ray diffractions were characterized with a diffractometer (Smart Lab-SE, Rigaku, Japan).

Chemical Synthesis. To show a proof of concept on the design of LLCs based on Pt(II) complexes, **Pt-3OC_nH_{2n+1}** ($n = 6, 12$ and 16) with a square-planar skeleton and three alkoxy tails was designed and synthesized (Scheme 1). 2-Methoxyethanol and H_2O (3/1 by volume) were mixed and used as the solvent, $\text{PtCl}_2(\text{DMSO})_2$

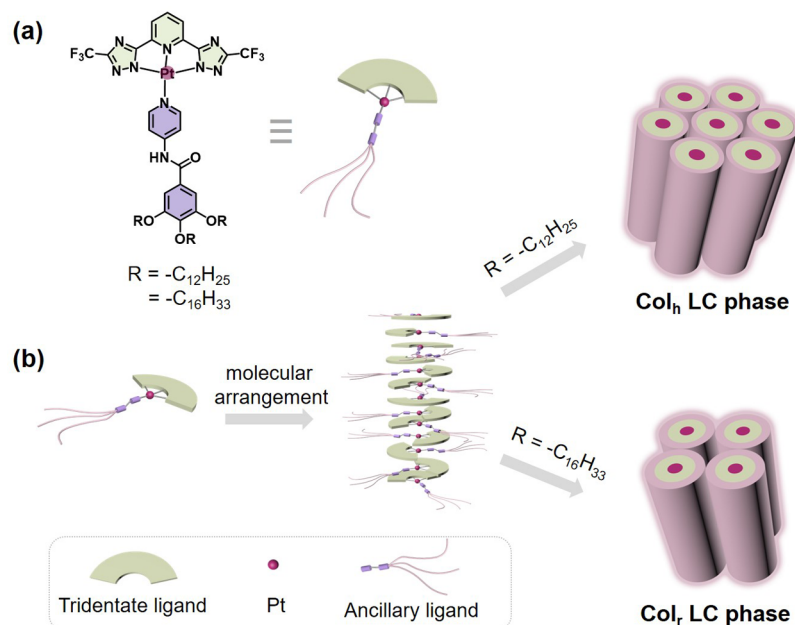


Figure 1. (a) Chemical structure and schematic representations of LLCs based on Pt(II) complexes. (b) Schematic illustration of the molecular arrangement of Pt(II) complexes, wherein hexagonal columnar (Col_h) and rectangular columnar (Col_r) LC phases are envisioned depending on the chain length on the ancillary ligand, respectively.

(DMSO = dimethylsulfoxide) was used as the Pt(II) precursor, and DIPEA was employed as the base. The skeleton consisted of a tridentate ligand [e.g., 2,6-bis(3-(trifluoromethyl)-1H-1,2,4-triazol-5-yl)pyridine] and an ancillary pyridine ligand with a substitution at the position 4. The tridentate ligand and PtCl₂(DMSO)₂ were synthesized according to the procedures reported by De Cola and co-workers³⁵ (see details in the Supporting Information), while the ancillary ligands with different chain lengths were synthesized through a sequential etherification and amidation procedures.²⁷

Synthesis of Methyl 3,4,5-Tris(hexyloxy)benzoate (1a). 1-Bromohexane (24.87 g, 81.46 mmol) was added into the stirred solution of methyl gallate (3.00 g, 16.29 mmol) and potassium carbonate (22.52 g, 162.91 mmol) in 2-butanone (100 mL) under the protection of nitrogen gas. After stirring under reflux for 24 h, solids were filtered-off and the filtrate was concentrated under vacuum that was subsequently purified by silica gel column chromatography. DCM and petroleum ether (1/1 by volume) were employed as the mobile phase. The product was obtained as pale yellow oil (yield: 91%). ¹H NMR (400 MHz, CDCl₃): δ 7.18 (s, 2H), 3.94 (td, 6H), 3.81 (s, 3H), 1.79–1.63 (m, 6H), 1.47–1.35 (m, 6H), 1.31–1.20 (m, 12H), 0.87–0.78 (m, 9H).

Synthesis of Methyl 3,4,5-Tris(dodecyloxy)benzoate (1b). The synthesis was similar to the preparation of 1a, and 1-bromododecane was employed as one reactant. The product was a white solid substance (yield: 89%). ¹H NMR (400 MHz, CDCl₃): δ 7.19 (s, 2H), 3.94 (td, 6H), 3.82 (s, 3H), 1.79–1.62 (m, 6H), 1.45–1.33 (m, 6H), 1.32–1.13 (m, 48H), 0.81 (t, 9H).

Synthesis of Methyl 3,4,5-Tris(hexadecyloxy)benzoate (1c). The synthesis was similar to the preparation of 1a and 1b, and 1-bromohexadecane was employed as one reactant. The product was a white solid substance (yield: 86%). ¹H NMR (400 MHz, CDCl₃): δ 7.18 (s, 2H), 3.94 (td, 6H), 3.82 (s, 3H), 1.76–1.64 (m, 6H), 1.52 (s, 6H), 1.42–1.37 (m, 6H), 1.23–1.16 (m, 66H), 0.81 (t, 9H).

Synthesis of the Ancillary Ligand 2a. 1a (2.00 g, 4.58 mmol) was dissolved together with 4-aminopyridine (0.47 g, 5.04 mmol) in anhydrous THF (20 mL), followed by slowly adding a solution of potassium *tert*-butanolate in anhydrous THF (2 mol/L, 2 mL). The mixture was stirred for 2 h, and then, the solvent was evaporated. The crude product was purified via column chromatography (silica, DCM: EtOH = 95/5 by volume), yielding a white solid substance (yield: 73%). ¹H NMR (400 MHz, CDCl₃): δ 8.45 (s, 2H), 8.16 (d, 1H),

7.54 (d, 2H), 6.97 (s, 2H), 3.93 (dt, 6H), 1.71 (m, 6H), 1.44–1.36 (m, 6H), 1.26 (dd, 12H), 0.83 (t, 9H). ESI-HR-MS (positive scan, *m/z*): [M + H]⁺, calcd 499.3530; found, 499.3529.

Synthesis of the Ancillary Ligand 2b. The preparation was similar to that of 2a, starting from 1b and yielding a white solid substance (yield: 55%). ¹H NMR (400 MHz, CDCl₃): δ 8.48 (d, 2H), 7.77 (s, 1H), 7.52 (d, 2H), 6.96 (s, 2H), 3.96 (q, 6H), 1.77–1.66 (m, 6H), 1.53 (s, 6H), 1.40 (dd, 6H), 1.19 (s, 42H), 0.81 (t, 9H). ESI-HR-MS (positive scan, *m/z*): [M + H]⁺, calcd 751.6347; found, 751.6344.

Synthesis of the Ancillary Ligand 2c. The preparation was similar to that of 2a and 2b, starting from 1c and yielding a white solid substance (yield: 52%). ¹H NMR (400 MHz, CDCl₃): δ 8.55 (d, 2H), 7.84 (s, 1H), 7.59 (d, 2H), 7.03 (s, 2H), 4.03 (td, 6H), 1.85–1.72 (m, 6H), 1.63 (s, 6H), 1.52–1.43 (m, 6H), 1.26 (s, 66H), 0.88 (t, 9H). ESI-HR-MS (positive scan, *m/z*): [M + H]⁺, calcd 919.8225; found, 919.8223.

Synthesis of Pt-3OC₆H₁₃, Pt-3OC₁₂H₂₅, and Pt-3OC₁₆H₃₃. The tridentate ligand (1.0 equiv), PtCl₂(DMSO)₂ (1.0 equiv), ancillary ligands (e.g., 2a, 2b, or 2c, 1.0 equiv), and 100 μL of DIPEA were added in 20 mL solvent of 2-methoxyethanol and H₂O (3/1 by volume). The reaction mixture was kept stirring overnight at 83 °C under the nitrogen gas atmosphere. After reaction, the target compound was obtained through column chromatography with silica gel as the stationary phase and DCM/EtOH (25/1 by volume) as the eluent. The final product was a yellow solid substance (yield: 70%).

Characterization of Pt-3OC₆H₁₃. ¹H NMR (400 MHz, CDCl₃): δ 8.84 (s, 2H), 8.54 (s, 1H), 7.81 (t, 1H), 7.39 (s, 4H), 7.00 (s, 2H), 3.97 (t, 2H), 3.89 (t, 4H), 1.78–1.71 (m, 6H), 1.51–1.41 (m, 6H), 1.34 (dd, 12H), 0.95–0.90 (m, 9H). ¹⁹F NMR (400 MHz, CDCl₃): δ -64.17. ¹³C NMR (400 MHz, CDCl₃): δ 165.88, 160.98, 152.32, 150.99, 150.39, 145.89, 145.45, 141.39, 141.11, 126.41, 119.53, 116.84, 115.87, 104.95, 72.48, 68.16, 30.74, 30.58, 29.34, 28.21, 24.72, 24.64, 21.68, 21.54, 13.07, 12.99. ESI-HR-MS (negative scan, *m/z*): [M - H]⁻, calcd 1038.3366; found, 1038.3347.

Characterization of Pt-3OC₁₂H₂₅. ¹H NMR (400 MHz, CDCl₃): δ 9.00 (s, 2H), 8.38 (s, 1H), 7.89 (t, 1H), 7.61–7.48 (m, 4H), 6.93 (s, 2H), 3.95 (t, 2H), 3.86 (t, 4H), 1.79–1.68 (m, 6H), 1.45 (dd, 6H), 1.28 (d, 48H), 0.89 (t, 9H). ¹⁹F NMR (400 MHz, CDCl₃): δ -64.08. ¹³C NMR (400 MHz, CDCl₃): δ 165.99, 160.89, 152.36, 151.05, 150.41, 145.86, 145.40, 141.44, 141.00, 126.32, 119.51, 116.83, 116.17, 104.92, 72.48, 68.15, 30.96, 28.83–28.61, 28.43–28.33,

25.18, 25.09, 21.71, 13.10. ESI-HR-MS (negative scan, m/z): $[M - H]^-$, calcd 1290.6183; found, 1290.6219.

Characterization of Pt-3OC₁₆H₃₃. ¹H NMR (400 MHz, CDCl₃): δ 8.98 (s, 2H), 8.53 (s, 1H), 7.87 (t, 1H), 7.56–7.46 (dd, 4H), 6.97 (s, 2H), 3.96 (t, 2H), 3.88 (t, 4H), 1.75 (m, 6H), 1.48–1.41 (td, 6H), 1.29 (d, 72H), 0.88 (t, 9H). ¹⁹F NMR (400 MHz, CDCl₃): δ –64.08. ¹³C NMR (400 MHz, CDCl₃): δ 166.15, 160.73, 152.36, 150.68, 150.27, 145.86, 145.31, 141.47, 141.01, 126.28, 119.48, 116.79, 116.29, 105.08, 72.48, 68.20, 30.96, 28.87–28.69, 28.42, 25.21, 25.13, 21.70, 13.10. ESI-HR-MS (negative scan, m/z): $[M - H]^-$, calcd 1458.8061; found, 1458.8036.

RESULTS AND DISCUSSION

Liquid Crystalline Properties. All the three designed Pt(II) complexes, that is, Pt-3OC₆H₁₃, Pt-3OC₁₂H₂₅, and Pt-3OC₁₆H₃₃, are stable upon heating up to 350 °C under the nitrogen atmosphere, according to the TGA analysis (Figure S26). Nonetheless, Pt-3OC₆H₁₃ is crystalline at room temperature and no LC phase is observed during heating and cooling (Figure S27), primarily due to the limited flexibility associated with the short tails on the ancillary ligand. By contrast, both Pt-3OC₁₂H₂₅ and Pt-3OC₁₆H₃₃ readily exhibit LC characteristics. We hypothesized that different LC phases (e.g., hexagonal and rectangular columnar LC phases) would be formed by Pt-3OC₁₂H₂₅ and Pt-3OC₁₆H₃₃, respectively, because different chain lengths on the ancillary ligand were expected to lead to different aggregation behaviors of the Pt(II) complexes (Figure 1).

POM images show that both Pt-3OC₁₂H₂₅ and Pt-3OC₁₆H₃₃ can exhibit LC phases. As shown in Figure 2,

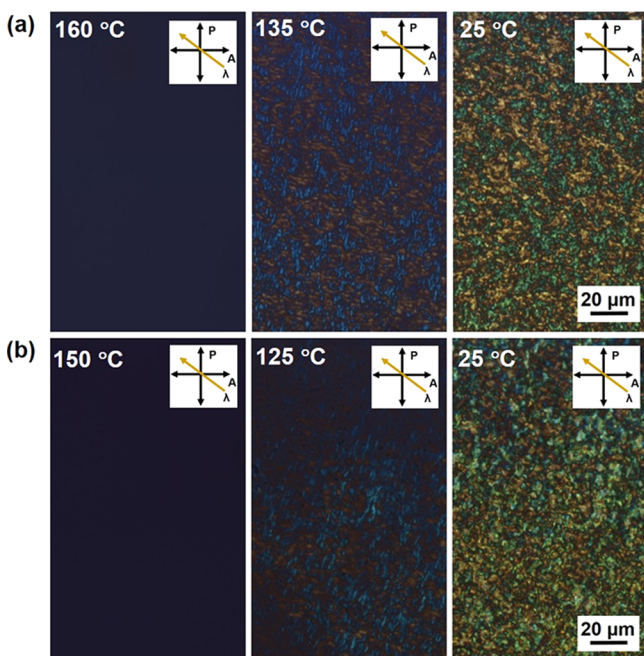


Figure 2. POM images of (a) Pt-3OC₁₂H₂₅ and (b) Pt-3OC₁₆H₃₃ when cooling from the isotropic state, respectively.

birefringence textures in the POM images can be observed when cooling the isotropic samples from high temperatures to the room temperature. Dark blue- and brown-polarized interference colors are observed at 135 °C under POM for Pt-3OC₁₂H₂₅, which turn to green and gold at 25 °C (Figure 2a), indicating changes of phase retardation that could be associated with a molecular rearrangement upon cooling.^{9,36}

Although green and gold colors are also observed at 25 °C for Pt-3OC₁₆H₃₃, cyan blue- and brown-polarized interference colors appear at a high temperature (125 °C, Figure 2b), which are different from those of Pt-3OC₁₂H₂₅. These colors can be correlated with different alignments of LC director relative to crossed polarizers of POM and are characteristics of such optically anisotropic mesophases with spatially varying director fields.

DSC results show that both Pt-3OC₁₂H₂₅ and Pt-3OC₁₆H₃₃ can show LC phases at room temperature. As shown in Figure 3a, there is one exothermic peak at 139 °C for Pt-3OC₁₂H₂₅ during the first run of cooling, which is ascribed to the liquid-mesophase transition in combination with the POM results. Upon heating, the mesophase-liquid transition peak shifts to 153 °C. Differently, one finds two exothermic peaks when cooling Pt-3OC₁₆H₃₃ from 180 to –30 °C, in which the peak at 129 °C is ascribed to the liquid-mesophase transition, while another peak at 15 °C may correspond to the crystallization of the hexadecyl chains (Figure 3b). This assumption is supported by the large enthalpy (24.1 J/g) during phase transition and the closer alkyl chain packing from 0.46 to 0.44 nm upon cooling by liquid nitrogen (Figure S28a). The crystallization of hexadecyl chain can show an enthalpy as large as 163 J/g (Figure S29). However, there is no change in the POM textures when cooling Pt-3OC₁₆H₃₃ by liquid nitrogen (Figure S28b). Upon heating, the low-temperature transition peak shifts to 22 °C and the mesophase-liquid transition peak shifts to 142 °C, respectively. Both the mesophase-liquid transition temperature and enthalpy are much smaller than those of the crystalline Pt-3OC₆H₁₃ during the melting because of the less ordered structures of LCs (Figure S27).

To probe the symmetry of the LC phases, 1D wide-angle X-ray diffraction (WAXD) and SAXS characterizations were performed. Figure 4 illustrates the 1D-WAXD results. As shown in the wide-angle region, the diffraction peak corresponds to a close intermolecular stacking of Pt-3OC₁₂H₂₅ with a d -spacing of 0.33 nm, which agrees well with the intermolecular distance of Pt(II) complexes reported by Yam and co-workers.³⁷ In addition, a broad halo is clear, which is indicative of the amorphous packing of alkyl chains. Although a diffraction peak corresponding to the intermolecular stacking is also observed in the 1D-WAXD pattern of Pt-3OC₁₆H₃₃, the packing of hexadecyl chains exhibits a diffraction peak rather than a typical halo at room temperature due to that the crystallization of hexadecyl chains can occur near the room temperature according to the DSC measurements. It is worth noting that there is another diffraction peak with a d -spacing of 1.05 and 1.06 nm in the WAXD patterns for Pt-3OC₁₂H₂₅ and Pt-3OC₁₆H₃₃, respectively, which implies the formation of ordered structures. However, the lattice parameters need to be further identified using SAXS analysis. As shown in Figure 5a, four diffraction peaks are clear in the small-angle region of SAXS patterns for Pt-3OC₁₂H₂₅, corresponding to the d -spacings (d_{hkl}) of 3.64, 2.10, 1.82, and 1.37 nm and being indexed to the (100), (110), (200), and (210) crystal planes based on eq 1, respectively. The hexagonal columnar (Col_h) LC phase is confirmed based on the reciprocal d -spacing ratio, that is, 1: $1/\sqrt{3}$: 1/2: $1/\sqrt{7}$,³⁸ and the lattice parameter a equals 4.20 nm.

$$1/d_{hkl}^2 = 4(h^2 + k^2 + hk)/3a^2 \quad (1)$$

where h , k , and l represent the Miller indices.

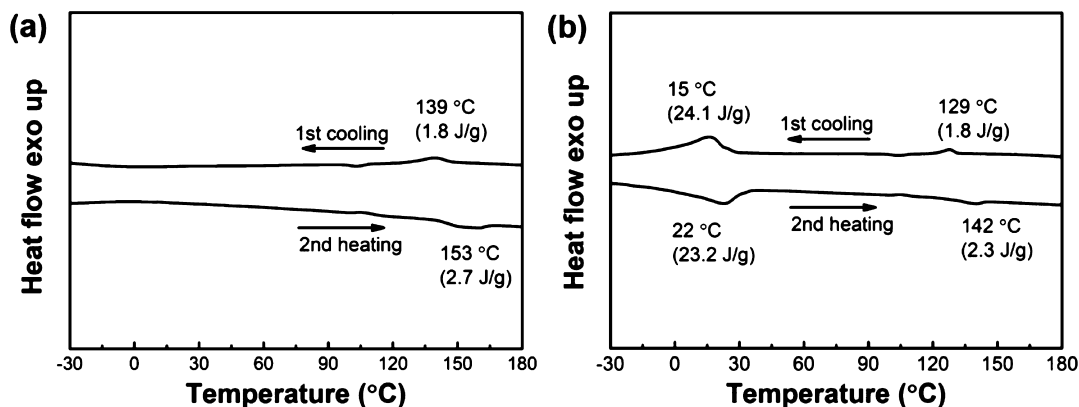


Figure 3. DSC curves of (a) Pt-3OC₁₂H₂₅ and (b) Pt-3OC₁₆H₃₃.

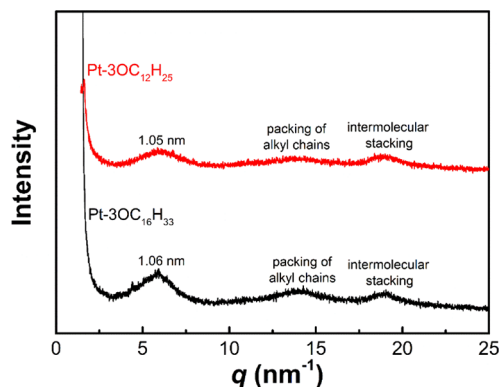


Figure 4. 1D-WAXD patterns of Pt-3OC₁₂H₂₅ and Pt-3OC₁₆H₃₃ at room temperature after first cooling.

By comparison, clearly distinct peaks are observed for Pt-3OC₁₆H₃₃ during the SAXS analysis (Figure 5b). Four diffraction peaks in the small-angle region are observed, corresponding to the *d*-spacings of 3.73, 3.23, 2.37, and 1.82 nm and being indexed to (100), (010), (110), and (200) crystal planes according to eq 2,³⁸ respectively. Thus, a rectangular columnar (Col_r) LC phase is confirmed, similar to how it was identified in previous reports³⁹ on the basis of the reciprocal *d*-spacing ratio, that is, 1:1/1.2:1/1.6:1/2. In addition, the lattice parameters, that is, *a* and *b* are calculated to be 3.73 and 3.23 nm, respectively, from the spacings of *d*₁₀₀ and *d*₀₁₀.

$$1/d_{hkl}^2 = h^2/a^2 + k^2/b^2 \quad (2)$$

Both Pt-3OC₁₂H₂₅ and Pt-3OC₁₆H₃₃ exhibit columnar LC phases due to that the square-planar geometry of Pt(II) complexes favors the molecular stacking in the aggregated states through intermolecular Pt··Pt and π - π interactions. However, distinct LC phases (i.e., Col_h and Col_r phases) are produced by modifying the complex core with different flexible peripheral alkoxy chains. The hexagonal packing array of Pt-3OC₁₂H₂₅ can be observed in most Pt(II) complexes which can form LC phases,^{3,33} metallogels⁴⁰ and supramolecular structures.⁴¹ Compared with Pt-3OC₁₂H₂₅, Pt-3OC₁₆H₃₃ with much longer flexible peripheral chains generates a different columnar LC phase with the rectangular packing lattice. The Pt-3OC₁₆H₃₃ molecules are unlikely to be coplanar because of the large steric perturbation by longer chains. To reach close packing and thus minimize the free energy, the long alkyl chains with increased internal freedom of rotation may extend in one direction when confined by the metal core, resulting in the formation of slanted columns, in favor of packing in the rectangular columnar phase.⁴² Similar LC phase transition behaviors have been reported by Kishikawa, Zhang, and co-workers.^{43,44}

Photophysical Properties. Photophysical properties of the Pt(II) complex-based LLCs are studied. As observed in other Pt(II) complexes reported by De Cola and co-workers^{26,27} and in the crystalline Pt-3OC₆H₁₃ (Figure S30), intense absorption of these LLCs peaked at 305 nm is clear in the UV wavelength region when dissolved in CH₂Cl₂ (Figure

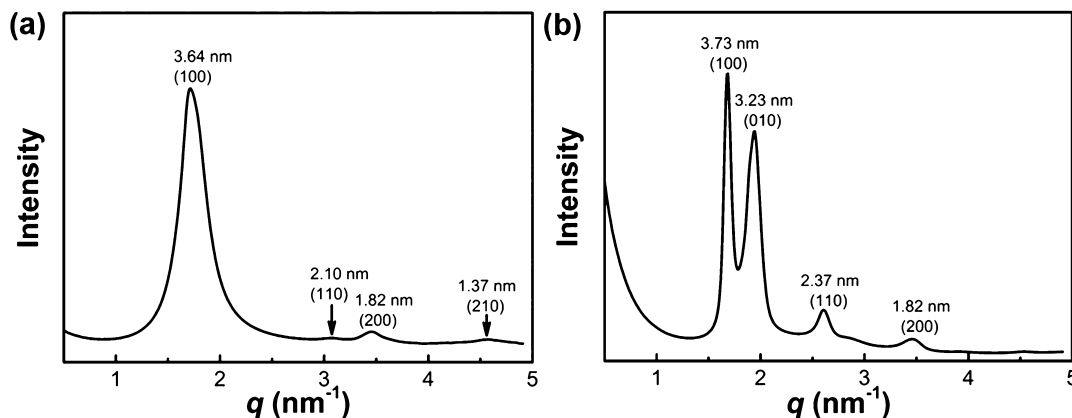


Figure 5. SAXS patterns of (a) Pt-3OC₁₂H₂₅ and (b) Pt-3OC₁₆H₃₃ at room temperature.

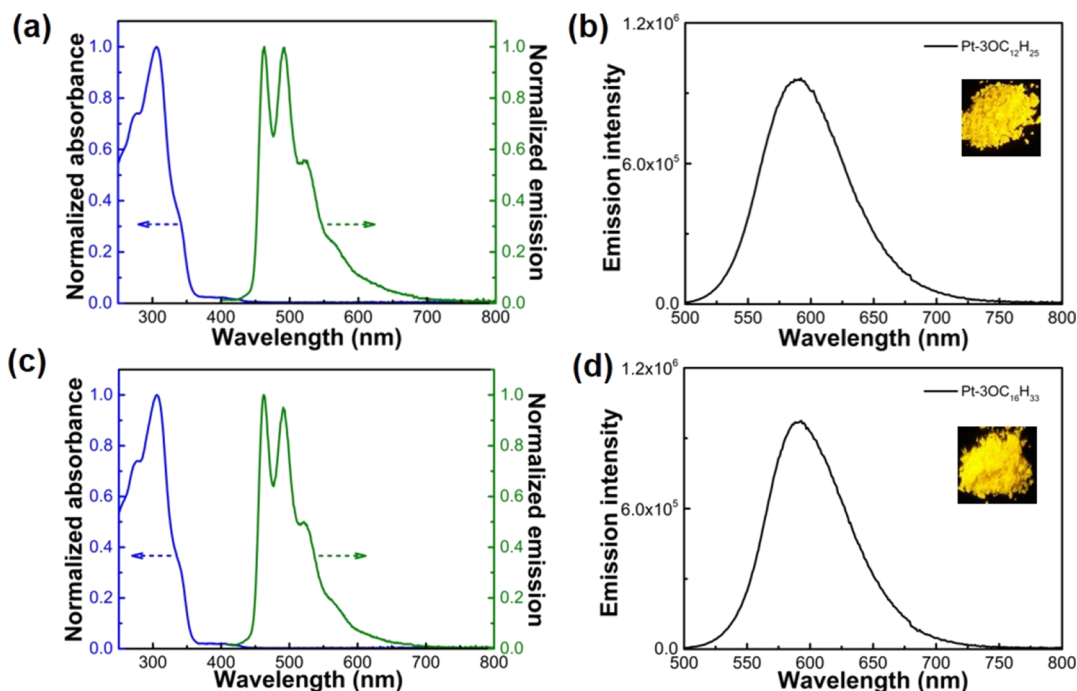


Figure 6. Absorption and emission spectra of (a) Pt-3OC₁₂H₂₅ and (c) Pt-3OC₁₆H₃₃ in CH₂Cl₂ (concentration: 10⁻⁵ M) at room temperature; emission spectra of (b) Pt-3OC₁₂H₂₅ and (d) Pt-3OC₁₆H₃₃ in powder. Excitation wavelength: 365 nm.

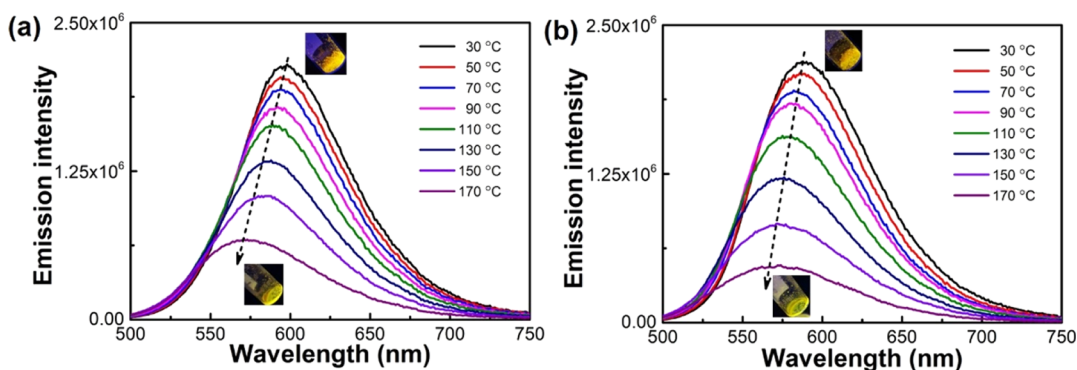


Figure 7. Emission intensity against temperature of (a) Pt-3OC₁₂H₂₅ and (b) Pt-3OC₁₆H₃₃ when excited by 365 nm UV light. Insets: LLCs in vials at room temperature and 170 °C under UV light, respectively.

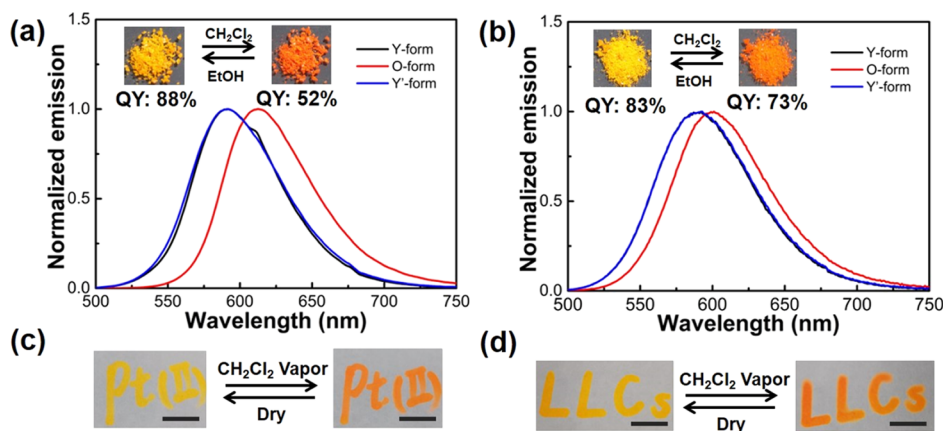


Figure 8. Emission spectra of (a) Pt-3OC₁₂H₂₅ and (b) Pt-3OC₁₆H₃₃ in different forms when fuming with CH₂Cl₂ and EtOH, respectively. Excitation wavelength: 365 nm. Inset: Color change under ambient light during the fuming process. (c,d) Reversible vapo-chromic patterns written on the filter paper and viewed under ambient light: (c) Pt-3OC₁₂H₂₅, (d) Pt-3OC₁₆H₃₃. Scale bars: 1 cm.

6a,c), which is mainly attributed to the intraligand (^1IL) and metal-perturbed interligand charge transfer ($^1\text{ILCT}$).²⁶ Besides, a broad absorption band in the wavelength region of 350–450 nm is noted, which can be assigned to the admixture of spin-allowed metal-to-ligand charge transfer ($^1\text{MLCT}$) and spin-forbidden $^3\text{MLCT}$.^{26,27,45} Upon photoexcitation, these LLCs show emissions at 463, 492, 524, and 568 nm (shoulder), respectively, which are attributed to the ligand-centered triplet excited state involving the tridentate chelate.^{26,45} Interestingly, a significantly redshifted emission is observed for these LLCs when aggregated (Figure 6b,d). The emission of $\text{Pt-3OC}_{12}\text{H}_{25}$ and $\text{Pt-3OC}_{16}\text{H}_{33}$ in aggregation peaks at 588 and 592 nm, respectively, gives rise to yellow color to their powder. These yellow color emissions can be ascribed to the MMLCT that is boosted by the $\text{Pt}\cdots\text{Pt}$ and $\pi\text{-}\pi$ stacking interactions.^{26,46} These $\text{Pt}\cdots\text{Pt}$ interactions can be verified by the newly generated intense emission peaked at 580 nm when increasing the complex concentration (Figure S31), in consistency with the reports from Che, Yam, De Cola, Wang and co-workers.^{47–50} Excitingly, these LLCs in aggregation exhibit a high QY, that is, 88% for $\text{Pt-3OC}_{12}\text{H}_{25}$ and 83% for $\text{Pt-3OC}_{16}\text{H}_{33}$, respectively. Besides, they show a relatively long photoluminescence lifetime, that is, 443 and 467 ns, respectively (Figure S32). It is worth noting that the photoluminescence QY and lifetime of the Pt(II) complexes are highly dependent on aggregation states and their environment.²⁷ Although the emission intensity is decreased upon heating, these LLCs can maintain their emission properties in the mesophase at high temperature (Figure 7).

Reversible Vaporchromism. These Pt(II) complexes show reversible vaporchromism, as previously reported for other Pt(II) complexes.^{51–53} When dried, they are yellow solid substances (referred to as Y-form) and exhibit yellow color emissions upon 365 nm light irradiation at room temperature. However, the emission color turns to orange within several minutes when the powder is exposed to the CH_2Cl_2 vapor (Figure 8a,b). The orange solid state is referred to as O-form. The redshift of the emission color is because of the reduced $\text{Pt}\cdots\text{Pt}$ distance in the presence of low molecular weight halohydrocarbons such as CH_2Cl_2 .^{30,52} It is reported that the CH_2Cl_2 molecules can enter into the crystal lattice of the complexes via $\text{C-H}(\text{CH}_2\text{Cl}_2)\cdots\pi$ interactions, resulting in a decrease of the $\text{Pt}\cdots\text{Pt}$ distance and HOMO–LUMO energy gap.^{52,54} The emission peak of $\text{Pt-3OC}_{12}\text{H}_{25}$ and $\text{Pt-3OC}_{16}\text{H}_{33}$ is significantly redshifted from 588 and 592 to 612 and 601 nm (Figure 8a,b) upon CH_2Cl_2 fuming, respectively, although the QY decreases from 88 and 83 to 52 and 73%. Compared with these LLCs, the crystalline $\text{Pt-3OC}_6\text{H}_{13}$ shows a larger redshift for 29 nm in emission (Figure S33). It seems that complexes with shorter chains are more sensitive to CH_2Cl_2 vapor, probably due to that the shorter side chains show less influence on the intermolecular stacking. Excitingly, the emission of all complexes can return to the original state upon EtOH fuming. This process is fully reversible for at least seven cycles (Figure S34). Powder WAXD analyses show that the d -spacing of the O-form powder is smaller, and the diffraction peaks are greater after treating the Y-form powder with CH_2Cl_2 vapor (Figure S35), indicating that the molecular packing of the complexes tends to be closer and more ordered.^{52–54} After fuming by EtOH, the Y-form is regenerated.

The reversible vaporchromism of these LLCs shows a great application potential in vapor sensing and anti-counterfeiting. For instance, reversible vaporchromic patterns (e.g., “Pt(II)”

and “LLCs”) can be achieved by writing the LLCs/ CH_2Cl_2 solution using a brush on the filter paper (Figure 8c,d). Color change from yellow to orange can be observed by fuming the patterns with CH_2Cl_2 for 10 s, which reverses upon drying in air. Such vaporchromism behavior has also been reported for many organometallic and coordination complexes.⁵¹ However, this is one report of the LLCs with both the high QY and the vaporchromism properties.

CONCLUSIONS

Highly efficient luminescent platinum(II) complexes were designed and synthesized, which exhibit an absolute QY up to 88%. $\text{Pt-3OC}_{12}\text{H}_{25}$ showed the Col_h LC phase, while $\text{Pt-3OC}_{16}\text{H}_{33}$ exhibited the Col_r LC phase via delicately modifying the complex core with different flexible peripheral alkoxy chains. These complexes exhibited reversible vaporchromic physical behaviors and maintained their emission properties in the mesophase at high temperature, showing a great potential to be applied in advanced anti-counterfeiting and vapor sensing.

ASSOCIATED CONTENT

Supporting Information

The Supporting Information is available free of charge at <https://pubs.acs.org/doi/10.1021/acsami.0c13935>.

Synthesis, characterization, and other experimental details (PDF)

AUTHOR INFORMATION

Corresponding Authors

Haiyan Peng – Key Lab for Material Chemistry of Energy Conversion and Storage, Ministry of Education, and National Anti-Counterfeit Engineering Research Center, School of Chemistry and Chemical Engineering, Huazhong University of Science and Technology, Wuhan 430074, China; orcid.org/0000-0002-0083-8589; Email: hypeng@hust.edu.cn

Xiaolin Xie – Key Lab for Material Chemistry of Energy Conversion and Storage, Ministry of Education, and National Anti-Counterfeit Engineering Research Center, School of Chemistry and Chemical Engineering, Huazhong University of Science and Technology, Wuhan 430074, China; orcid.org/0000-0001-5097-7416; Email: xlxie@hust.edu.cn

Authors

Xingtian Hao – Key Lab for Material Chemistry of Energy Conversion and Storage, Ministry of Education, and National Anti-Counterfeit Engineering Research Center, School of Chemistry and Chemical Engineering, Huazhong University of Science and Technology, Wuhan 430074, China

Bijin Xiong – Key Lab for Material Chemistry of Energy Conversion and Storage, Ministry of Education, and National Anti-Counterfeit Engineering Research Center, School of Chemistry and Chemical Engineering, Huazhong University of Science and Technology, Wuhan 430074, China

Mingli Ni – Key Lab for Material Chemistry of Energy Conversion and Storage, Ministry of Education, and National Anti-Counterfeit Engineering Research Center, School of Chemistry and Chemical Engineering, Huazhong University of Science and Technology, Wuhan 430074, China

Bing Tang – State Key Laboratory of Materials Processing and Die & Mould Technology, School of Materials Science and Engineering, Huazhong University of Science and Technology, Wuhan 430074, China; orcid.org/0000-0001-8379-3453

Ying Ma – State Key Laboratory of Materials Processing and Die & Mould Technology, School of Materials Science and Engineering, Huazhong University of Science and Technology, Wuhan 430074, China; orcid.org/0000-0002-5649-7410

Xingping Zhou – Key Lab for Material Chemistry of Energy Conversion and Storage, Ministry of Education, and National Anti-Counterfeit Engineering Research Center, School of Chemistry and Chemical Engineering, Huazhong University of Science and Technology, Wuhan 430074, China

Ivan I. Smalyukh – Department of Physics and Materials Science and Engineering Program, University of Colorado at Boulder, Boulder, Colorado 80309, United States; orcid.org/0000-0003-3444-1966

Complete contact information is available at:
<https://pubs.acs.org/10.1021/acsami.0c13935>

Notes

The authors declare no competing financial interest.

ACKNOWLEDGMENTS

This work is financially supported by the NSFC (51773073, 51903097, 52073108, and 51433002) and peak boarding program (HUST). The technical assistance from the HUST Analytical & Testing Center and Core Facilities of Life Sciences is appreciated. We thank Prof. Zhen Li at Wuhan University for helping with the measurements of the photoluminescence quantum yield and lifetime. The use of the beamline BL16B1 at Shanghai Synchrotron Radiation Facility (SSRF) is also gratefully appreciated.

REFERENCES

- (1) Zhao, D.; Fan, F.; Cheng, J.; Zhang, Y.; Wong, K. S.; Chigrinov, V. G.; Kwok, H. S.; Guo, L.; Tang, B. Z. Light-Emitting Liquid Crystal Displays Based on an Aggregation-Induced Emission Luminogen. *Adv. Opt. Mater.* **2015**, *3*, 199–202.
- (2) De, J.; Yang, W.-Y.; Bala, I.; Gupta, S. P.; Yadav, R. A. K.; Dubey, D. K.; Chowdhury, A.; Jou, J.-H.; Pal, S. K. Room-Temperature Columnar Liquid Crystals as Efficient Pure Deep-Blue Emitters in Organic Light-Emitting Diodes with an External Quantum Efficiency of 4.0%. *ACS Appl. Mater. Interfaces* **2019**, *11*, 8291–8300.
- (3) Lu, W.; Chen, Y.; Roy, V. A. L.; Chui, S. S.-Y.; Che, C.-M. Supramolecular Polymers and Chromonic Mesophases Self-Organized from Phosphorescent Cationic Organoplatinum(II) Complexes in Water. *Angew. Chem., Int. Ed.* **2009**, *48*, 7621–7625.
- (4) Hu, Y.-X.; Hao, X.; Xu, L.; Xie, X.; Xiong, B.; Hu, Z.; Sun, H.; Yin, G.-Q.; Li, X.; Peng, H.; Yang, H.-B. Construction of Supramolecular Liquid-Crystalline Metallacycles for Holographic Storage of Colored Images. *J. Am. Chem. Soc.* **2020**, *142*, 6285–6294.
- (5) Peng, H.; Bi, S.; Ni, M.; Xie, X.; Liao, Y.; Zhou, X.; Xue, Z.; Zhu, J.; Wei, Y.; Bowman, C. N.; Mai, Y.-W. Monochromatic Visible Light “Photoinitiator”: Janus-Faced Initiation and Inhibition for Storage of Colored 3D Images. *J. Am. Chem. Soc.* **2014**, *136*, 8855–8858.
- (6) Chen, G.; Ni, M.; Peng, H.; Huang, F.; Liao, Y.; Wang, M.; Zhu, J.; Roy, V. A. L.; Xie, X. Photoinitiation and Inhibition under Monochromatic Green Light for Storage of Colored 3D Images in Holographic Polymer-Dispersed Liquid Crystals. *ACS Appl. Mater. Interfaces* **2017**, *9*, 1810–1819.
- (7) Zhao, Y.; Zhao, X.; Li, M. D.; Li, Z. A.; Peng, H.; Xie, X. Crosstalk-Free Patterning of Cooperative-Thermoresponse Images by

the Synergy of the AIEgen with the Liquid Crystal. *Angew. Chem., Int. Ed.* **2020**, *59*, 10066–10072.

(8) Zhao, X.; Sun, S.; Zhao, Y.; Liao, R.-Z.; Li, M.-D.; Liao, Y.; Peng, H.; Xie, X. Effect of Ketyl Radical on the Structure and Performance of Holographic Polymer/Liquid-Crystal Composites. *Sci. China Mater.* **2019**, *62*, 1921–1933.

(9) Peng, H.; Yu, L.; Chen, G.; Xue, Z.; Liao, Y.; Zhu, J.; Xie, X.; Smalyukh, I. I.; Wei, Y. Liquid Crystalline Nanocolloids for the Storage of Electro-Optic Responsive Images. *ACS Appl. Mater. Interfaces* **2019**, *11*, 8612–8624.

(10) Levitsky, I. A.; Kishikawa, K.; Eichhorn, S. H.; Swager, T. M. Exciton Coupling and Dipolar Correlations in a Columnar Liquid Crystal: Photophysics of a Bent-Rod Hexacatenar Mesogen. *J. Am. Chem. Soc.* **2000**, *122*, 2474–2479.

(11) Ting, C.-H.; Chen, J.-T.; Hsu, C.-S. Synthesis and Thermal and Photoluminescence Properties of Liquid Crystalline Polyacetylenes Containing 4-Alkanyloxyphenyl Trans-4-Alkylcyclohexanoate Side Groups. *Macromolecules* **2002**, *35*, 1180–1189.

(12) Luo, J.; Xie, Z.; Lam, J. W. Y.; Cheng, L.; Tang, B. Z.; Chen, H.; Qiu, C.; Kwok, H. S.; Zhan, X.; Liu, Y.; Zhu, D. Aggregation-Induced Emission of 1-Methyl-1,2,3,4,5-Pentaphenylsilole. *Chem. Commun.* **2001**, 1740–1741.

(13) Mei, J.; Leung, N. L. C.; Kwok, R. T. K.; Lam, J. W. Y.; Tang, B. Z. Aggregation-Induced Emission: Together We Shine, United We Soar! *Chem. Rev.* **2015**, *115*, 11718–11940.

(14) Li, Q.; Li, Z. The Strong Light-Emission Materials in the Aggregated State: What Happens from a Single Molecule to the Collective Group. *Adv. Sci.* **2017**, *4*, 1600484.

(15) Chen, L.; Chen, C.; Sun, Y.; Lu, S.; Huo, H.; Tan, T.; Li, A.; Li, X.; Ungar, G.; Liu, F.; Zhang, M. Luminescent Metallacycle-Cored Liquid Crystals Induced by Metal Coordination. *Angew. Chem., Int. Ed.* **2020**, *59*, 10143–10150.

(16) Liu, Y.; You, L. H.; Lin, F. X.; Fu, K.; Yuan, W. Z.; Chen, E.-Q.; Yu, Z.-Q.; Tang, B. Z. Highly Efficient Luminescent Liquid Crystal with Aggregation-Induced Energy Transfer. *ACS Appl. Mater. Interfaces* **2019**, *11*, 3516–3523.

(17) Wang, Y.; Liao, Y.; Cabry, C. P.; Zhou, D.; Xie, G.; Qu, Z.; Bruce, D. W.; Zhu, W. Highly Efficient Blueish-Green Fluorescent OLEDs Based on AIE Liquid Crystal Molecules: From Ingenious Molecular Design to Multifunction Materials. *J. Mater. Chem. C* **2017**, *5*, 3999–4008.

(18) Tao, L.; Li, M.-L.; Yang, K.-P.; Guan, Y.; Wang, P.; Shen, Z.; Xie, H.-L. Color-Tunable and Stimulus-Responsive Luminescent Liquid Crystalline Polymers Fabricated by Hydrogen Bonding. *ACS Appl. Mater. Interfaces* **2019**, *11*, 15051–15059.

(19) Zhu, J.-C.; Han, T.; Guo, Y.; Wang, P.; Xie, H.-L.; Meng, Z.-G.; Yu, Z.-Q.; Tang, B. Z. Design and Synthesis of Luminescent Liquid Crystalline Polymers with “Jacketing” Effect and Luminescent Patterning Applications. *Macromolecules* **2019**, *52*, 3668–3679.

(20) Kim, D.-Y.; Koo, J.; Lim, S.-I.; Jeong, K.-U. Solid-State Light Emission Controlled by Tuning the Hierarchical Superstructure of Self-Assembled Luminogens. *Adv. Funct. Mater.* **2018**, *28*, 1707075.

(21) Mu, B.; Zhao, Y.; Li, X.; Quan, X.; Tian, W. Enhanced Conductivity and Thermochromic Luminescence in Hydrogen Bond-Stabilized Columnar Liquid Crystals. *ACS Appl. Mater. Interfaces* **2020**, *12*, 9637–9645.

(22) Zhu, Y.; Zheng, M.; Tu, Y.; Chen, X.-F. Supramolecular Fluorescent Polymers Containing A-Cyanostilbene-Based Stereoisomers: Z/E-Isomerization Induced Multiple Reversible Switching. *Macromolecules* **2018**, *51*, 3487–3496.

(23) Chen, Y.; Lin, J.; Yuan, W.; Yu, Z.; Lam, J. W.; Tang, B. Z. 1-((12-Bromododecyl)Oxy)-4-((4-(4-Pentylcyclohexyl)Phenyl)-Ethynyl) Benzene: Liquid Crystal with Aggregation-Induced Emission Characteristics. *Sci. China: Chem.* **2013**, *56*, 1191–1196.

(24) Wan, J.-H.; Mao, L.-Y.; Li, Y.-B.; Li, Z.-F.; Qiu, H.-Y.; Wang, C.; Lai, G.-Q. Self-Assembly of Novel Fluorescent Silole Derivatives into Different Supramolecular Aggregates: Fibre, Liquid Crystal and Monolayer. *Soft Matter* **2010**, *6*, 3195–3201.

- (25) Guo, L.-X.; Xing, Y.-B.; Wang, M.; Sun, Y.; Zhang, X.-Q.; Lin, B.-P.; Yang, H. Luminescent Liquid Crystals Bearing an Aggregation-Induced Emission Active Tetraphenylthiophene Fluorophore. *J. Mater. Chem. C* **2019**, *7*, 4828–4837.
- (26) Carrara, S.; Aliprandi, A.; Hogan, C. F.; De Cola, L. Aggregation-Induced Electrochemiluminescence of Platinum(II) Complexes. *J. Am. Chem. Soc.* **2017**, *139*, 14605–14610.
- (27) Sinn, S.; Yang, L.; Biedermann, F.; Wang, D.; Kübel, C.; Cornelissen, J. J. L. M.; De Cola, L. Templated Formation of Luminescent Virus-Like Particles by Tailor-Made Pt(II) Amphiphiles. *J. Am. Chem. Soc.* **2018**, *140*, 2355–2362.
- (28) Aliprandi, A.; Mauro, M.; De Cola, L. Controlling and Imaging Biomimetic Self-Assembly. *Nat. Chem.* **2016**, *8*, 10–15.
- (29) Yam, V. W.-W.; Au, Y. K.-M.; Leung, S. Y.-L. Light-Emitting Self-Assembled Materials Based on d^8 and d^{10} Transition Metal Complexes. *Chem. Rev.* **2015**, *115*, 7589–7728.
- (30) Ni, J.; Wu, Y.-H.; Zhang, X.; Li, B.; Zhang, L.-Y.; Chen, Z.-N. Luminescence Vapochromism of a Platinum(II) Complex for Detection of Low Molecular Weight Halohydrocarbon. *Inorg. Chem.* **2009**, *48*, 10202–10210.
- (31) Kozhevnikov, V. N.; Donnio, B.; Bruce, D. W. Phosphorescent, Tridentate, Liquid-Crystalline Complexes of Platinum(II): Stimulus-Dependent Emission. *Angew. Chem., Int. Ed.* **2008**, *47*, 6286–6289.
- (32) Cuerva, C.; Campo, J. A.; Cano, M.; Lodeiro, C. Multi-Stimuli-Responsive Properties of Aggregation-Enhanced Emission-Active Unsymmetrical Pt(II) Metallomesogens through Self-Assembly. *Chem.—Eur. J.* **2019**, *25*, 12046–12051.
- (33) Camerel, F.; Ziesel, R.; Donnio, B.; Bourgoigne, C.; Guillon, D.; Schmutz, M.; Iacovita, C.; Bucher, J.-P. Formation of Gels and Liquid Crystals Induced by Pt··Pt and π - π^* Interactions in Luminescent σ -Alkynyl Platinum(II) Terpyridine Complexes. *Angew. Chem., Int. Ed.* **2007**, *46*, 2545.
- (34) Krikorian, M.; Liu, S.; Swager, T. M. Columnar Liquid Crystallinity and Mechanochromism in Cationic Platinum(II) Complexes. *J. Am. Chem. Soc.* **2014**, *136*, 2952–2955.
- (35) Mydlak, M.; Mauro, M.; Polo, F.; Felicetti, M.; Leonhardt, J.; Diener, G.; De Cola, L.; Strassert, C. A. Controlling Aggregation in Highly Emissive Pt(II) Complexes Bearing Tridentate Dianionic $N^A N^A N$ Ligands. Synthesis, Photophysics, and Electroluminescence. *Chem. Mater.* **2011**, *23*, 3659–3667.
- (36) Gim, M.-J.; Beller, D. A.; Yoon, D. K. Morphogenesis of Liquid Crystal Topological Defects During the Nematic-Smectic a Phase Transition. *Nat. Commun.* **2017**, *8*, 15453.
- (37) Wong, V. C.-H.; Po, C.; Leung, S. Y.-L.; Chan, A. K.-W.; Yang, S.; Zhu, B.; Cui, X.; Yam, V. W.-W. Formation of 1D Infinite Chains Directed by Metal-Metal and/or π - π Stacking Interactions of Water-Soluble Platinum(II) 2,6-Bis(benzimidazol-2'-yl)pyridine Double Complex Salts. *J. Am. Chem. Soc.* **2018**, *140*, 657–666.
- (38) Laschat, S.; Baro, A.; Steinke, N.; Giesselmann, F.; Hägele, C.; Scalia, G.; Judele, R.; Kapatsina, E.; Sauer, S.; Schreivogel, A.; Tosoni, M. Discotic Liquid Crystals: From Tailor-Made Synthesis to Plastic Electronics. *Angew. Chem., Int. Ed.* **2007**, *46*, 4832–4887.
- (39) Zhu, Y.-F.; Guan, X.-L.; Shen, Z.; Fan, X.-H.; Zhou, Q.-F. Competition and Promotion between Two Different Liquid-Crystalline Building Blocks: Mesogen-Jacketed Liquid-Crystalline Polymers and Triphenylene Discotic Liquid Crystals. *Macromolecules* **2012**, *45*, 3346–3355.
- (40) Chan, M. H.-Y.; Ng, M.; Leung, S. Y.-L.; Lam, W. H.; Yam, V. W.-W. Synthesis of Luminescent Platinum(II) 2,6-Bis(N-dodecylbenzimidazol-2'-yl)pyridine Foldamers and Their Supramolecular Assembly and Metallogel Formation. *J. Am. Chem. Soc.* **2017**, *139*, 8639–8645.
- (41) Zhang, K.; Yeung, M. C.-L.; Leung, S. Y.-L.; Yam, V. W.-W. Manipulation of Nanostructures in the Co-Assembly of Platinum(II) Complexes and Block Copolymers. *Chem* **2017**, *2*, 825–839.
- (42) Xu, Y.-S.; Shi, D.; Gu, J.; Lei, Z.; Xie, H.-L.; Zhao, T.-P.; Yang, S.; Chen, E.-Q. Synthesis and Self-Organization of Azobenzene Containing Hemiphasmidic Side-Chain Liquid-Crystalline Polymers with Different Spacer Lengths. *Polym. Chem.* **2016**, *7*, 462–473.
- (43) Kishikawa, K.; Nakahara, S.; Nishikawa, Y.; Kohmoto, S.; Yamamoto, M. A Ferroelectrically Switchable Columnar Liquid Crystal Phase with Achiral Molecules: Superstructures and Properties of Liquid Crystalline Ureas. *J. Am. Chem. Soc.* **2005**, *127*, 2565–2571.
- (44) Wang, J.; Zhang, C.; Zhang, S.; Hao, X.; Hong, F.; Zhang, A.; Wang, Y.-F.; Wu, H.; Zhang, W.; Pu, J.-L. A Systematic Study on the Influences of Linkage Length on Phase Behaviours and Charge Carrier Mobilities of Discotic Dimers. *Liq. Cryst.* **2017**, *44*, 394–404.
- (45) Mauro, M.; Aliprandi, A.; Cebrián, C.; Wang, D.; Kübel, C.; De Cola, L. Self-Assembly of a Neutral Platinum(II) Complex into Highly Emitting Microcrystalline Fibers through Metallophilic Interactions. *Chem. Commun.* **2014**, *50*, 7269–7272.
- (46) Meng, W.; He, Q.; Yu, M.; Zhou, Y.; Wang, C.; Yu, B.; Zhang, B.; Bu, W. Telechelic Amphiphilic Metallopolymers End-Functionalized with Platinum(II) Complexes: Synthesis, Luminescence Enhancement, and Their Self-Assembly into Flowerlike Vesicles and Giant Flowerlike Vesicles. *Polym. Chem.* **2019**, *10*, 4477–4484.
- (47) Tsai, J. L.-L.; Zou, T.; Liu, J.; Chen, T.; Chan, A. O.-Y.; Yang, C.; Lok, C.-N.; Che, C.-M. Luminescent Platinum(II) Complexes with Self-Assembly and Anti-Cancer Properties: Hydrogel, pH Dependent Emission Color and Sustained-Release Properties under Physiological Conditions. *Chem. Sci.* **2015**, *6*, 3823–3830.
- (48) Chan, M. H.-Y.; Leung, S. Y.-L.; Yam, V. W.-W. Rational Design of Multi-Stimuli-Responsive Scaffolds: Synthesis of Luminescent Oligo(Ethynylpyridine)-Containing Alkynylplatinum(II) Polypyridine Foldamers Stabilized by Pt··Pt Interactions. *J. Am. Chem. Soc.* **2019**, *141*, 12312–12321.
- (49) Liu, L.; Wang, X.; Wang, N.; Peng, T.; Wang, S. Bright, Multi-Responsive, Sky-Blue Platinum(II) Phosphors Based on a Tetradentate Chelating Framework. *Angew. Chem., Int. Ed.* **2017**, *56*, 9160–9164.
- (50) Chakraborty, S.; Aliprandi, A.; De Cola, L. Multinuclear Pt(II) Complexes: Why Three is Better than Two to Enhance Photophysical Properties. *Chem.—Eur. J.* **2020**, *26*, 11007–11012.
- (51) Wenger, O. S. Vapochromism in Organometallic and Coordination Complexes: Chemical Sensors for Volatile Organic Compounds. *Chem. Rev.* **2013**, *113*, 3686–3733.
- (52) Jiang, B.; Zhang, J.; Ma, J.-Q.; Zheng, W.; Chen, L.-J.; Sun, B.; Li, C.; Hu, B.-W.; Tan, H.; Li, X.; Yang, H.-B. Vapochromic Behavior of a Chair-Shaped Supramolecular Metallacycle with Ultra-Stability. *J. Am. Chem. Soc.* **2016**, *138*, 738–741.
- (53) Soto, M. A.; Carta, V.; Andrews, R. J.; Chaudhry, M. T.; MacLachlan, M. J. Structural Elucidation of Selective Solvatochromism in a Responsive-at-Metal Cyclometalated Platinum(II) Complex. *Angew. Chem., Int. Ed.* **2020**, *59*, 10348–10352.
- (54) Kui, S. C. F.; Chui, S. S.-Y.; Che, C.-M.; Zhu, N. Structures, Photoluminescence, and Reversible Vapoluminescence Properties of Neutral Platinum(II) Complexes Containing Extended π -Conjugated Cyclometalated Ligands. *J. Am. Chem. Soc.* **2006**, *128*, 8297–8309.